THE JOURNAL OF PHYSICAL CHEMISTRY B

Article

pubs.acs.org/JPCB

Simulations Reveal Conformational Changes of Methylhydroxyl Groups during Dissolution of Cellulose I_β in Ionic Liquid 1-Ethyl-3-methylimidazolium Acetate

Hanbin Liu,[†,‡] Gang Cheng,[†,‡] Michael Kent,[†,§] Vitalie Stavila,[‡] Blake A Simmons,[†,‡] Kenneth L Sale,[†,‡] and Seema Singh*[,†,‡]

[†]Deconstruction Division, Joint BioEnergy Institute, Emeryville, California

[‡]Sandia National Laboratories, Livermore, California

[§]Sandia National Laboratories, Albuquerque, New Mexico

Supporting Information

ABSTRACT: In this work, we use molecular dynamics (MD) simulations to study the dissolution of microcrystalline cellulose in the ionic liquid 1-ethyl-3-methylimidazolium acetate (abbreviated as [C2mim][OAc]) at 20 wt % loading. The interactions of [C_2mim][OAc] with the I_β cellulose structure at 120 °C were studied. The results show that both the cation and the anion of [C_2mim][OAc] penetrate into the cellulose I_β crystal structure but that the anion in particular forms strong hydrogen bonds with cellulose. Our results also show that the methylhydroxyl groups of cellulose solvated in [C_2mim][OAc] are predominantly in the gauche−trans (gt) conformation, in contrast to the dominant trans−gauche (tg) conformation of cellulose I_β in air or the gauche−gauche (gg) conformation for cellulose chains in water or after pretreatment with ammonia. Because the gt conformation is found mainly in cellulose II, these simulations suggest that regenerated cellulose under similar pretreatment conditions is composed mainly of cellulose II, and this result was confirmed by X-ray diffraction of samples processed under similar pretreatment conditions. These simulations provide new insight into the efficacy of [C_2mim][OAc] pretreatment, suggesting that [C_2mim][OAc] interacts with and biases the methylhydroxyl groups of cellulose toward orientations that are consistent with the experimentally observed more easily hydrolyzed cellulose II.

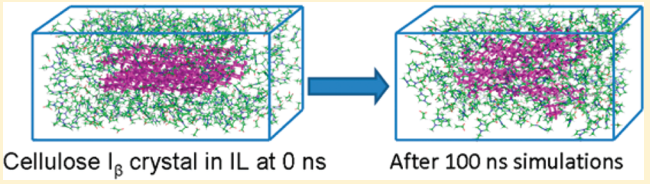

INTRODUCTION

The continued and increasing consumption of fossil resources worldwide, and a growing awareness of their contribution to global climate change, have motivated research for new products and process technologies that are low carbon, renewable and sustainable.[1] One major direction is to produce advanced biofuels using the polysaccharides found in plant cell walls of nonfood lignocellulose as a source of fermentable sugars.[1,2] The microcrystalline nature of native cellulose found in secondary plant cell walls requires energy to efficiently liberate fermentable sugars. In the native state, cellulose exists as a microcrystalline polymer, and the crystalline domains form two distinct polymorphs of cellulose I: I_α with a triclinic unit cell and I_β with a monoclinic unit cell, whose fractional distributions vary among plants of different origin.[3,4] Cellulose I_β was used in our study because cellulose I_β is the most abundant crystalline form of cellulose in plants and is thermodynamically more stable than cellulose I_α.[5]

Imidazolium-based ionic liquids (ILs), such as 1-ethyl-3-methylimidazolium acetate (abbreviated as [C_2mim][OAc]), dissolve significant amounts of microcrystalline cellulose and represent a class of solvent that is capable of overcoming the crystalline recalcitrance of cellulose I.[6−9] The dissolved cellulose can be recovered using either water or ethanol as an antisolvent.[6] This process generates amorphous cellulose, the polymorph cellulose II, or mixtures of the two that can be hydrolyzed by cellulases much more efficiently than cellulose I.[6−8,10−12] Initial results using ILs on microcrystalline cellulose have prompted researchers to pretreat and fractionate lignocellulosic biomass using ILs[9,13−16] into its cellulose, hemicelluloses and lignin[17−20] components to generate polysaccharides that can be easily hydrolyzed into fermentable sugars.

Despite the increasing number of ILs known to be capable of solvating microcrystalline cellulose,[9,13−16] the exact mechanism of how ILs interact with plant cell walls that are comprised of cellulose, hemicelluloses, and lignin remains unknown.[21] Given that there are over 10 000 different ILs and only 22−30 ILs have been shown to effectively dissolve cellulose, a fundamental understanding of the interactions of ionic liquids with cellulose on different length scales would enable design of ionic liquids with even stronger performance characteristics. A recent computer simulation study suggests both the shape of the cellulose microfibril and the cellulose polymorph contribute to

Received: February 20, 2012
Revised: May 7, 2012
Published: May 10, 2012

   dx.doi.org/10.1021/jp301673h | J. Phys. Chem. B 2012, 116, 8131−8138

biomass recalcitrance.[22] Rheological studies suggest that the dissolved cellulose chains in dilute solutions of [C_2mim][OAc] are not in an expanded state as they would be in a good solvent, suggesting that [C_2mim][OAc] may be closer to a theta solvent than a good solvent for cellulose.[23] With increasing cellulose concentration, it has been reported that individual chains interact to form liquid crystalline phases at 10 wt % and a gel phase at 12.5 wt % in [C_2mim][OAc].[24]

The mechanism of IL solvation of microcrystalline cellulose has been hypothesized to involve the strong hydrogen bond interactions that occur between [C_2mim][OAc] and cellulose that disrupt the intermolecular hydrogen bonds within the microfibril.[6] Several key publications from Rogers and Moyna investigate using NMR methods the effect of cation and anion when dissolving cellulose.[25−27] However the details of the dissolution mechanism remain controversial. Zhang et al. using NMR to investigate the interactions of glucose units and cellulose chains with ILs have shown that both the anions and cations form hydrogen bonds with the hydroxyl groups of cellulose.[28] Various computational methods, such as molecular dynamics (MD) simulations,[29,30] COSMO-RS,[31] and quantum mechanical calculations,[32] have been used to study the interaction of carbohydrates with solvents such as water and ILs. Molecular structures of microfibrils[33−36] and associated hydration shells in the presence of ILs and water have also been studied using computational simulations. A very recent study by Gross et al. used molecular dynamics simulations to study cellulose solvation in 1-butyl-3-methylimidazolium chloride.[36] More recently, Bellesia et al.[37] used molecular dynamics simulations to analyze cellulose I_β interacting with ammonia to model the early events associated with liquid ammonia pretreatment. Liu et al.[29] studied the interaction energy between [C_2mim][OAc] and cellulose and compared it with the interactions of cellulose with mixtures of water and organic solvent and determined that the cation interacts with cellulose chains mainly through hydrophobic interactions.

In this work, we use MD simulations to study the molecular level interactions between microcrystalline cellulose I_β and [C_2mim][OAc]. Conformational analysis was performed on the simulated system, and a relationship between the conformations of the different cellulose crystal polymorphs is proposed. When exposed to [C_2mim][OAc] at 20 wt % both the inter- and intrachain hydrogen bonds of cellulose I_β are very quickly disrupted (100 ns), which is due to $[OAc]^-$ forming hydrogen bonds with the hydroxyl groups of cellulose, and $[C2mim]^+$ making hydrophobic contacts with the cellulose chains. This mechanism agrees well with Rogers and Moyna's experimental findings,[25−27] as well as our earlier simulations of polysaccharide chains in the presence of [C_2mim][OAc]. Interestingly we also find that the side chain distributions of cellulose are altered dramatically from cellulose I_β to the solvated state in [C_2mim][OAc] solution where they are in favor of forming the cellulose II crystal, assuming the cellulose regeneration process is under kinetic control. We validated the MD results with XRD experiments on regenerated cellulose from the pretreatment of Avicel at 20 wt % loading and 120 °C. The experimental results confirmed that the regenerated materials are composed of cellulose II crystal and amorphous material.

METHODS

Microcrystalline Cellulose I Model. The molecular model of microcrystalline cellulose I_β was constructed based on the crystal symmetry and the atomic coordinates of cellulose I_β reported previously.[38] The cellulose I_β structure was reported to be a monoclinic crystal with P_{21} symmetry, and a unit-cell dimension of a = 7.784 Å, b = 8.201 Å, and c = 10.380 Å and r = 96.5°. This information was used as input to Pymol[39] to generate a microcrystal composed of 3 layers with 3 cellulose chains in each layer. The degree of polymerization (DP) of each glucose chain is 6, giving a total of 54 glucose units in our microcrystalline I_β model. Cellulose I_β has two chains labeled as the central and original chains. The structure of the simulated cellulose microcrystal, as well as the unit cell axes and the crystal surfaces are shown in Figure 1a,b. The size of our

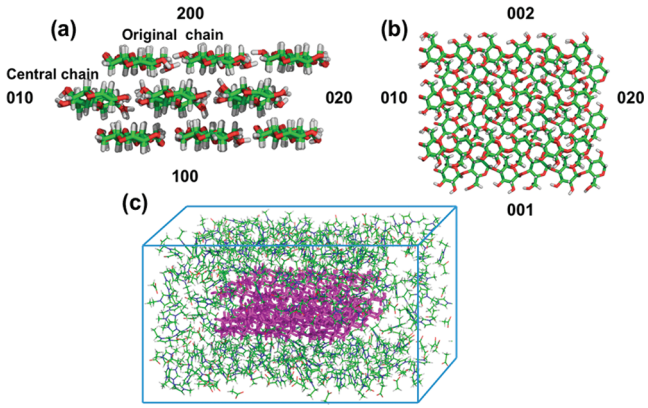

Figure 1. Images depicting the systems evaluated in the current work, (a) lateral view of cellulose I_β crystal, (b) normal view of cellulose I_β crystal orientation, and (c) unit volume of cellulose I_β crystal in [C_2mim][OAc].

cellulose system is quite small compared to an actual cellulose microfibril, but our model system retains all of the key interactions in the cellulose structure.

Since the positions of hydroxyl hydrogen atoms are not determined from X-ray diffraction data, we assigned the H coordinate based on the amber force field H-bond definition (instead of the favorable H-bond pattern described by Nishiyama, et al.[40]) To let the hydroxyl group dihedrals relax to favorable positions, the cellulose structure was first energy minimized by performing 500 steps of steepest decent followed by 1000 steps of conjugate gradient energy minimization and 1 ns of MD simulation with a restraint of 100 kcal/mol/Å on all heavy atoms. To analyze the H-bond pattern in the crystal structures, 40 ns MD simulations were performed on cellulose I_β in the NVT ensemble at 300 K, with a small restraint of 0.3 kcal/mol/Å on all heavy atoms to avoid the finite-size effect of the length of cellulose chains.

Cellulose I_β Dissolved in Ionic Liquid. The cellulose crystal was placed in a [C_2mim][OAc] solvent box (Figure 1c). The system was calculated to have 20 wt % cellulose in the cellulose-IL solution. The dimensions of the solvent box, composed of 220 [C_2mim][OAc] molecules, were set at 34 Å by 48 Å by 52 Å. The Packmol[41] program was used to generate the IL solvated system.

Force Field and MD Simulation. MD simulations were implemented in AMBER[42] using an all atom force field based on the generalized AMBER force field (GAFF)[43] for [C_2mim]-[OAc][29] and the carbohydrate force field, GLYCAM06,[44] for cellulose. The cutoff radius for nonbonded interactions was set to 12 Å. The Particle Mesh Ewald summation method[45] was used to calculate the electrostatic potential with periodic

dx.doi.org/10.1021/jp301673h | J. Phys. Chem. B 2012, 116, 8131−8138

boundary conditions. The initial configurations were energy minimized using the steepest descent algorithm for 1000 steps to remove any unexpected coordinate collisions. The systems were then heated for 200 ps in the NVT ensemble, during which the temperature was increased gradually to the target temperature, followed by a further 500 ps of equilibration dynamics in the NPT ensemble using the Nose-Hoover constant pressure (P = 1 bar) control algorithm at 120 °C. Finally, 100 ns production runs were carried out in the NPT ensemble. The time step for production runs was 2 fs and the SHAKE algorithm was employed to constrain bonds and angles involving hydrogen atoms. The last 90 ns of each trajectory were used for analysis.

XRD Measurement. 20% Avicel (PH101, Sigma Aldrich) was mixed with 1-ethyl-3-methyl imidazolium acetate (90%, Sigma Aldrich) and the mixture was kept at 120 °C for 1 h. Water was then added to the solution to precipitate the dissolved cellulose and the regenerated cellulose was washed extensively with water to remove the ionic liquid. It was then dried by lyophilization for further analysis. Powder X-ray diffraction (XRD) measurements were performed on a PANalytical Empyrean system equipped with a PIXcel^{3D} detector. The Bragg−Brentano geometry comprises a Cu X-ray tube (operated at 45 kV and 40 mA; λ = 1.5418 Å), incident beam optics with a 1/8° fixed divergence and a 1/4° antiscatter slit, as well as a 0.04 rad soller slit and receiving optics which include another 0.04 rad soller slit, a Ni K_β filter and the PIXcel^{3D} detector in scanning mode. A reflection-transmission spinner was used as a sample holder and the spinning rate was set at 8 rpm throughout the experiment. The patterns were collected in the 2θ range of 5 to 65°, the step size was 0.026°, and the exposure time was 300 s.

RESULTS AND DISCUSSION

To better understand the dominant interactions that determine the crystal packing of cellulose and to provide a baseline for examining changes in these interactions in the [C_2mim][OAc] environment, we first performed MD simulations in vacuo where nonbonding interactions are at their maximum strength. The intermolecular hydrogen bonds are the dominant interactions that stabilize the I_β stucture.[38,40] Nishiyama et al.[40] have shown that the O2 secondary alcohol and O6 hydroxymethyl groups are involved in both intra- and interchain H bonds within a sheet. Based on the H atoms covalently bound to the O6 and O2 atoms of glucose there are two dynamically interconvertible hydrogen bond networks (pattern A and pattern B as depicted in ref 37) that include both intra- and interchain hydrogen bonds within the same sheet. As the actual coordinates of the H atoms are not defined in X-ray diffraction data, to avoid starting the simulation in pure pattern A or pattern B, as described in the Methods section, we used the AMBER program to add the missing hydrogen atoms, energy minimized the resulting cellulose I_β crystal, and then allowed the hydrogen atoms to relax to favorable positions. The simulated unit cell parameters agree well with the measured crystal structure and indicate that the crystal structure is stable in our simulation system using the GLYCAM06 force field. The rmsd of the cellulose system (9 chains with 54 glucose unit) was calculated by aligning to the heavy atoms in the first frame of the simulations and the results are shown in Figure 2. The low rmsd (less than 0.7 Å) confirms that our crystal model is stable in the GLYCAM06 force field and thus accurately represents the crystal structure.

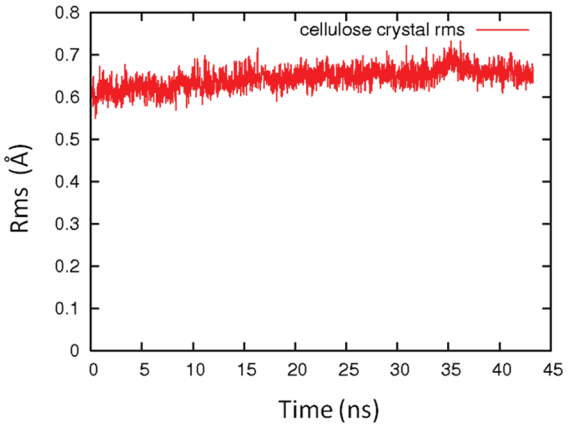

Figure 2. Calculated rms plot of the simulated crystal cellulose crystal I_β.

We investigated the dissolution of the cellulose crystal in [C_2mim][OAc] by comparing the numbers of both intra- and interchain hydrogen bonds between the simulation of the crystal form and the simulation in the ionic liquid solution. For the system with 9 chains and 54 glucose units in the cellulose I_β crystalline form, the maximum possible number of intrachain hydrogen bonds is 45, and the maximum possible number of interchain hydrogen bonds is 36. We defined hydrogen bonds as having an O···O distance less than 3.5 Å and an O−H···O angle larger than 150° and counted their number across the MD trajectory (Figure 3).

In the cellulose crystal simulation, the O3−H−O5 intrachain H bond is very precisely located with over 92% occupancy for all trajectories saved during the 40 ns simulations (Figure 3a). The O2−H−O6 is less defined and the average hydrogen bond occupancy in the equilibrium state was ∼45% (Figure 3b). Panels c and d in Figure 3 present the interchain hydrogen bonds. O6−H−O2 is dominant with a calculated occupancy of ∼88% at the equilibrium state, whereas the interchain hydrogen bond involved at O3 and O6 has an occupancy of 40%. When the cellulose crystal was dissolved in ionic liquid, our simulation results show that the number of interchain hydrogen bonds decreased significantly over the 100 ns simulation, and the occupancy of the interchain hydrogen bonds (both O6−H−O2 and O6−H−O3 bonds, Figure 4c,d) decreased to less than 2%. The intrachain interaction of the O3−H−O5 hydrogen bond occupancy decreased from 98% to 15% (Figure 3a) after mixing with [C_2mim][OAc], and the O2−H−O6 bond occupancy decreased to less than 5% (Figure 3b). This clearly demonstrates that the initial hydrogen bond network that defined and stabilized the microcrystalline cellulose was significantly disrupted in the presence of [C_2mim][OAc].

One of the key parameters defining the structure of cellulose crystals is the orientation of the O2−H−O6 hydrogen bond, which determined the position of the hydroxymethyl group C6−OH (Figure 4). The position of the hydroxymethyl group is defined by the O5−C5−C6−O6 and C4−C5−C6−O dihedral angles, which have three stable staggered rotamer conformations (Figure 4a): gauche−trans (gt), trans−gauche (tg), and gauche−gauche (gg). Because of the tetrahedral nature of C sp3 hybridization, $\omega = \omega^* + 120°$, the single torsion angle (C5−C6−O6−H6) specifies the orientation of the hydroxyl group of the side chain. Figure 4a illustrates the three major rotamer conformations and their corresponding torsion angle ω. The torsion angle (ω) of all the cellulose units

dx.doi.org/10.1021/jp301673h | J. Phys. Chem. B 2012, 116, 8131−8138

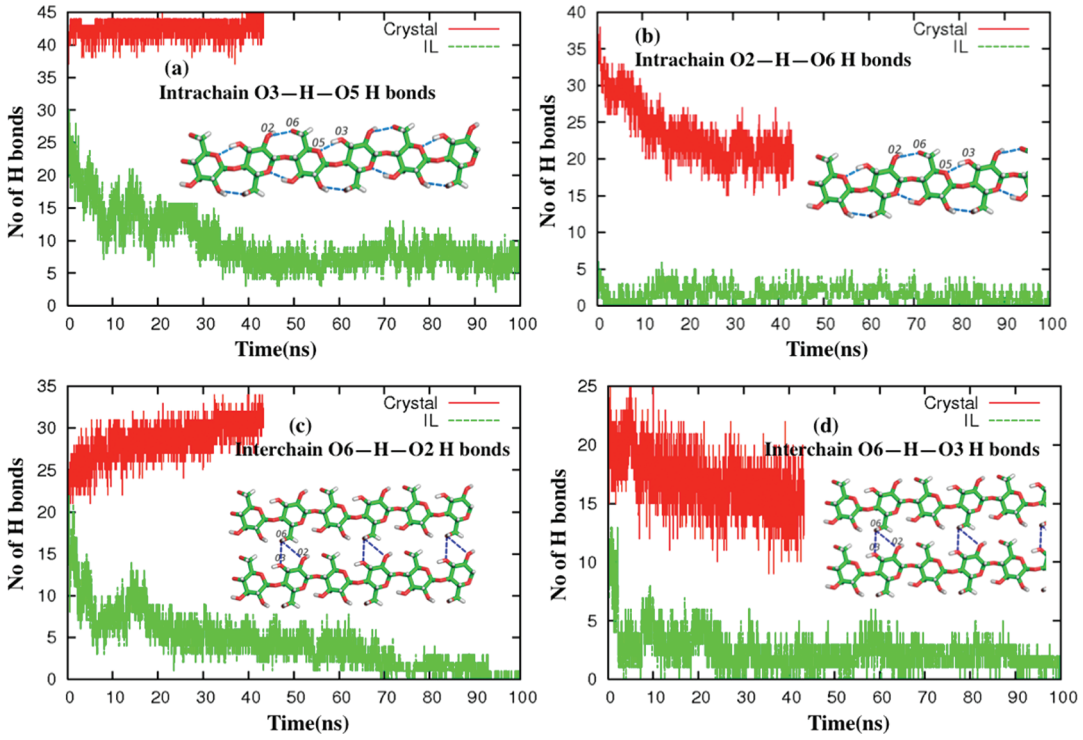

Figure 3. Number of four major H bonds in cellulose crystal and cellulose in IL solution simulations. (a) Intrachain O3−H−O5, (b) intrachain O2−H−O6, (c) interchain O6−H−O2, and (d) interchain O6−H−O3.

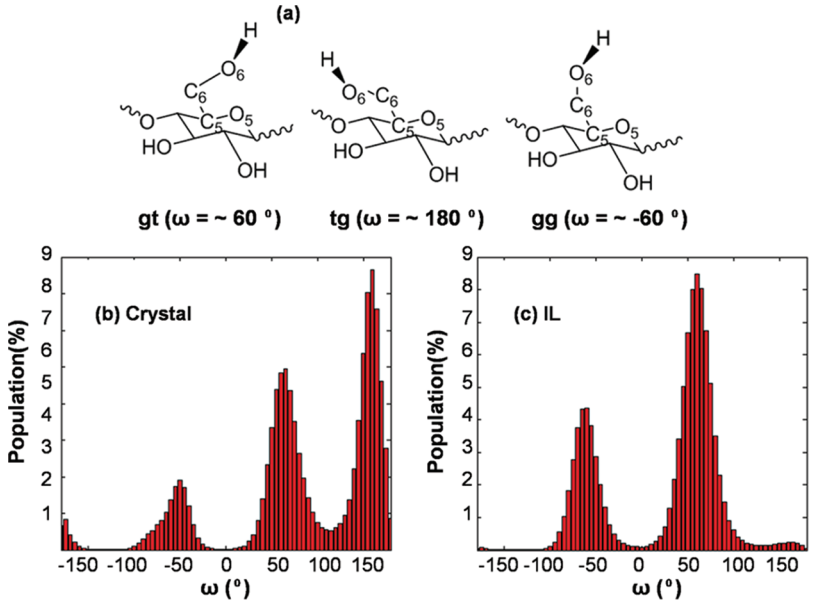

Figure 4. (a) Methyl hydroxyl group in sugar conformation and the calculated hydroxyl group orientation in the (b) crystal cellulose I_β in vacuum and (c) cellulose I_β in [C2mim][OAc] solution.

during our MD simulations was calculated and plotted as histograms (Figure 4b and 4c.) As shown in Figure 4b, the distribution of torsion angles present in the I_β protofibrils is tg > gt > gg. These results are in agreement with Langan[38,46] who showed that in both cellulose I_β and I_α, the tg conformation is preferred and confers formation of the O2−O6 hydrogen bond. Our simulations of the cellulose crystal dissolved in [C_2mim]-[OAc] solution, however, show a very different distribution of the torsion angle (Figure 4c). The main conformation of methyl hydroxyl groups in the IL solution is gt, with some gg conformations also being observed. The tg conformation, which is dominant in cellulose I_β (Figure 4b), was found to be less than 1% in the cellulose − [C_2mim][OAc] solution. The conformation of this methyl hydroxyl group plays an important role in determining the crystal packing of cellulose. Several computational studies[30,47] show that the preferred conformation of the methylhydroxyl group in aqueous solution is the gg conformation followed by gt conformation, while the tg conformation is least preferred. A change in the methylhydroxl group rotational state from tg to gt and gg was previously

dx.doi.org/10.1021/jp301673h | J. Phys. Chem. B 2012, 116, 8131−8138

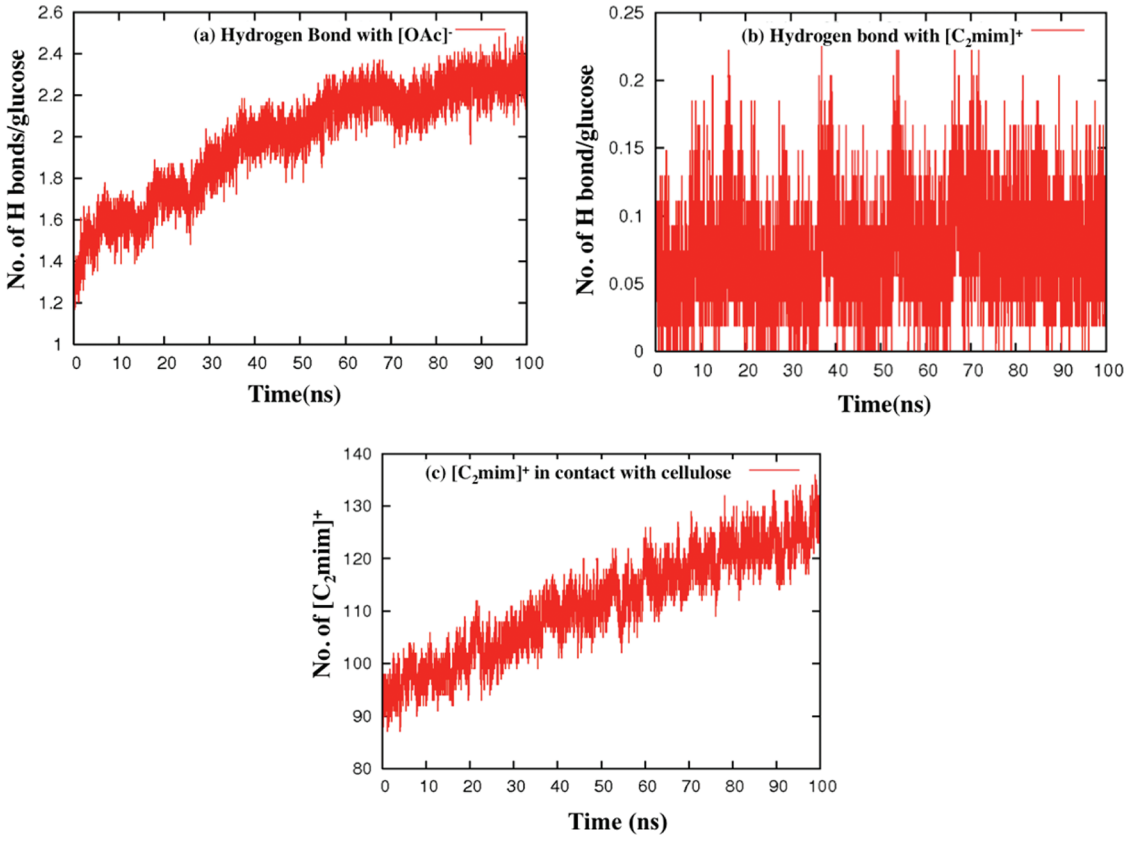

Figure 5. Number of hydrogen bonds formed with [C2mim][OAc], (a) with anion $[OAc]^-$, and (b) with cation $[C2mim]^+$. (c) number of cations $[C2mim]^+$ in contact with cellulose during dissolution.

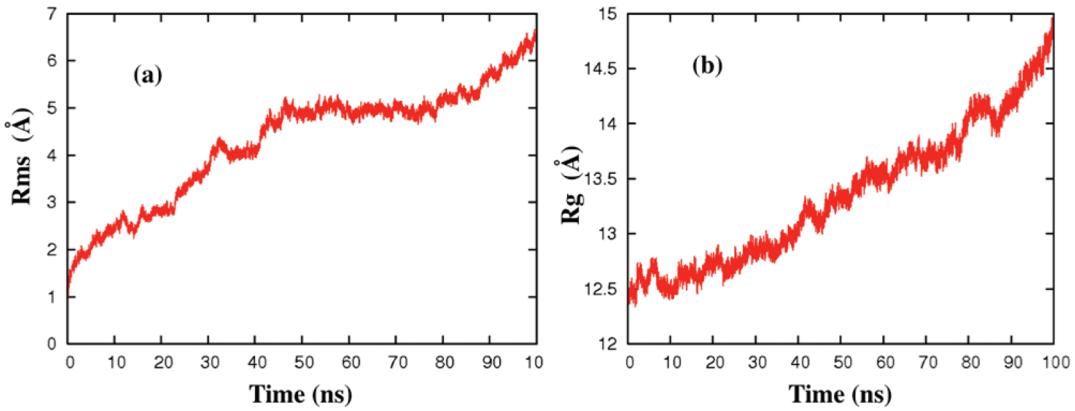

Figure 6. (a) Rms deviation and (b) radius of gyration of cellulose during dissolution.

observed in a simulation of liquid ammonia pretreatment of native crystalline cellulose.[37] That work[37] demonstrated that the gg conformation is the most populated rotational state and facilitated the transition from cellulose I_β to cellulose III. In contrast, when dissolved in $[C_2mim][OAc]$, the present work shows that the methylhydroxyl group distribution is different from that in ammonia exposed cellulose[37] (different distribution of gt and gg) as well as from that of the native cellulose crystal.

The time course of hydrogen bonds formed among the $[OAc]^-$ and the three free hydroxyl groups in each cellulose unit was calculated across the dissolution trajectory (Figure 5a). Dissolution of the cellulose I_β crystal occurs rapidly, and the average number of hydrogen bonds between the $[OAc]^-$ and the I_β crystal increases during the simulation. After 100 ns, ~80% of the hydroxyl groups of cellulose have formed hydrogen bonds with $[OAc]^-$, which we hypothesize to be the primary driver for dissolution. In addition to the formation of hydrogen bonds with $[OAc]^-$, we calculated the interactions of the acidic hydrogen, positioned between the two nitrogen atoms on the imidazolium ring, with cellulose. The results (Figure 5b) indicate that the formation of hydrogen bonds between $[C_2mim]^+$ and cellulose was minimal and did not change over the 100 ns simulation. Thus hydrogen bonding between the cation and cellulose was not a dominant force during dissolution, but may play a role in disrupting the crystal structure by diffusing into the cellulose and/or stabilizing the cellulose chains in solution.

dx.doi.org/10.1021/jp301673h | J. Phys. Chem. B 2012, 116, 8131−8138

To more fully define the role of $[C_2mim]^+$ during cellulose dissolution, we calculated the number of molecules in close proximity (within 3.5 Å) to the crystal (Figure 5c). The number of cations in contact with cellulose increased throughout the entire 100 ns simulation, reaching a maximum of over 135 $[C_2mim]^+$ cations in close contact with the cellulose crystal comprised of 54 glucose units. These results combined with visual inspections of the simulated trajectory indicate that the $[C_2mim]^+$ cations diffuse into the I_β lattice. These observations lead us to believe that cations play a role in the dissolution process through hydrophobic interactions.

The cellulose I_β crystal structure has a very distinct feature compared to cellulose II and III.[46] While cellulose II and III crystals are held together by strong intersheet hydrogen bonds, cellulose I_β does not have these hydrogen bonds, suggesting that hydrophobic interactions or other nonbonding interactions stabilize the cellulose I_β structure. Therefore we conclude that $[C_2mim]^+$ cations interact with cellulose through hydrophobic interactions that disrupt the ordered intersheet interactions present in cellulose I_β and play an important role in the solvation process.

In addition to the hydrogen bonding analysis, the process of swelling and dissolution of the cellulose in $[C_2mim][OAc]$ was monitored by measuring the root-mean-square deviation (rmsd) and the radius of gyration (R_g) of the cellulose crystal (Figure 6). R_g was calculated for the cellulose aggregate (9 chains with 54 glucose units) and rmsd was calculated by aligning all the heavy atoms to the original crystal conformation. Both rmsd and R_g increased during the simulations (Figure 6a,b). The increase in R_g over the length of the simulation indicates that the cellulose crystal swells during $[C_2mim][OAc]$ solvation. Diffusion of $[C_2mim][OAc]$ into the lattice of cellulose I_β occurs rapidly, evidenced by changes in both rmsd and R_g. After the initial solvation the rmsd plateaued at between 40 and 80 ns but the R_g values continued to increase. This phenomenon and our visual inspections of trajectories indicate that the cellulose crystal is swollen but the topology remains relatively constant (the chains are still parallel to each other) within 40 ns. During the simulations of 40−80 ns, the exposed cellulose chains started to tilt locally. This kind of conformation changes associated with dissolution did not have a large effect on the calculated rmsd but increased the R_g of the aggregate (see the illustration in Supporting Materials). After 80 ns, the system is further disrupted and results in partial solvation in $[C_2mim][OAc]$.

A recently revised structure of cellulose II from neutron fiber diffraction shows that both central and original chains (Figure 1a) have gauche (gt) conformations.[46] Cellulose can be regenerated from solution in IL by adding water as an antisolvent.[6] If regeneration of cellulose upon water addition is a kinetically controlled step, some of the cellulose chains can aggregate and precipitate before the methylhydroxyl groups respond to the water environment and transform to the gg conformation or to the tg conformation to regenerate cellulose I. In other words, the gt or gg conformation should dominate in the regenerated cellulose. Because the majority of the side chain conformation is gt in cellulose II and gg in amorphous cellulose, it is expected that regenerated cellulose will consist of a mixture of cellulose II and amorphous cellulose.

Previously, Cheng et al.[48] demonstrated the conversion of cellulose I polymorph to a mixture of cellulose II and amorphous cellulose upon IL pretreatment at a loading of 3 wt %. The present MD simulations were carried out for a more industrially relevant loading of 20 wt %. Therefore, in order to confirm whether our MD simulation results agree with experimental results under similar conditions and loading, cellulose (Avicel) at 20 wt % was incubated in $[C_2mim][OAc]$ at 120 °C for 1 h, followed by addition of hot water (~85 °C) to the solution to precipitate the cellulose. The regenerated cellulose was washed extensively with water and freeze-dried for 24 h. Powder XRD was used to study the crystalline structure of the regenerated cellulose. Figure 7 presents powder XRD

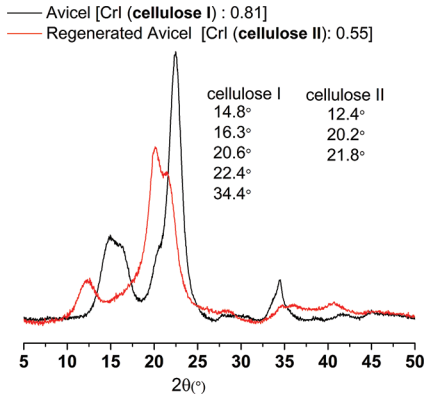

Figure 7. XRD spectrum of untreated Avicel and regenerated Avicel after $[C_2mim][OAc]$ treatment at 120 °C for 1 h.

data of both untreated and $[C_2mim][OAc]$ treated Avicel. The spectrum of untreated Avicel is consistent with that of cellulose I with characteristic peaks at 14.8°, 16.3°, 20.6°, 22.4°, and 34.4°,[49] but a determination of the fraction of I_α or I_β is difficult for powder samples.[50] The crystallinity index (CrI) of cellulose I, estimated by comparing the area of the sample spectrum to that of amorphous cellulose, was 0.81.[51] In contrast, the XRD spectrum of the regenerated cellulose has peaks at 12.4°, 20.2°, and 21.8°, which is consistent with the spectrum of cellulose II. The CrI of cellulose II was estimated to be 0.55. These experimental results confirm that the regenerated materials are composed of cellulose II and amorphous cellulose, in agreement with our expectations based on the simulation results. We note that these results help to explain the differences in enzymatic hydrolysis efficiency that have been reported for cellulose pretreated via ammonia and IL, since pretreatment by ammonia leads to mainly cellulose III.[37]

■ CONCLUSION

In this work, we used molecular dynamics simulations to study the dissolution of a model cellulose I_β crystal in the ionic liquid $[C_2mim][OAc]$. Our results show that $[C_2mim][OAc]$ extensively disrupts the cellulose lattice: the cellulose I_β crystal experiences substantial swelling and the methylhydroxyl side chains of glucose reorient from their preferred trans−gauche conformation in the cellulose I_β crystal to a predominantly gauche−trans rotamer state. Our simulations also showed that these disruptions in the cellulose fiber are due to strong interactions of both the anion and the cation with cellulose. The anion forms strong hydrogen bonds with hydroxyl groups of the sugar units, whereas the imidazolium ring of the cation interacts with the sugar groups through hydrophobic and ring−ring interactions, disrupting the cellulose I_β intersheet interactions.

We also examined changes in the cellulose crystal structure after incubation in $[C_2mim][OAc]$ followed by addition of

dx.doi.org/10.1021/jp301673h | J. Phys. Chem. B 2012, 116, 8131−8138

water as the antisolvent using powder X-ray diffraction (XRD) measurements. The XRD data confirm the conversion of cellulose I into a mixture of cellulose II and amorphous cellulose under the same conditions as used in the MD simulations.

Based on these data our current working model for the dissolution of cellulose by $[C_2mim][OAc]$ and subsequent formation of a mixture of cellulose II and amorphous cellulose upon addition of an antisolvent is that the anion and cation of $[C_2mim][OAc]$ interact strongly with the cellulose I fiber, disrupting its structure and priming it to take on a new structural form. Upon addition of water the methyl hydroxyl groups are trapped in these new orientations, because their reorientation time is slow compared to the time scale of cellulose repacking as the IL is washed out of the fiber.

■ ASSOCIATED CONTENT

Supporting Information

Representative picture of cellulose dissolution in 1-ethyl-3-methyl imidazolium acetate during our MD simulations (Figure S1). This material is available free of charge via the Internet at http://pubs.acs.org.

■ AUTHOR INFORMATION

Corresponding Author

*E-mail: seesing@sandia.gov. Phone: 510-495-2490. Fax: (510) 486-4252.

Notes

The authors declare no competing financial interest.

■ ACKNOWLEDGMENTS

This work was part of the DOE Joint BioEnergy Institute (http://www.jbei.org) supported by the U.S. Department of Energy, Office of Science, Office of Biological and Environmental Research, through Contract DE-AC02-05CH11231 between Lawrence Berkeley National Laboratory and the U.S. Department of Energy. This research used resources of the National Energy Research Scientific Computing Center (NERSC).

■ REFERENCES

(1) Himmel, M. E.; Ding, S. Y.; Johnson, D. K.; Adney, W. S.; Nimlos, M. R.; Brady, J. W.; Foust, T. D. *Science* **2007**, *315*, 804.
(2) Simmons, B. A.; Loque, D.; Blanch, H. W. *Genome Biol.* **2008**, *9*, 242.
(3) Sugiyama, J.; Persson, J.; Chanzy, H. *Macromolecules* **1991**, *24*, 2461.
(4) Kono, H.; Yunoki, S.; Shikano, T.; Fujiwara, M.; Erata, T.; Takai, M. *J. Am. Chem. Soc.* **2002**, *124*, 7506.
(5) Yamamoto, H.; Horii, F.; Odani, H. *Macromolecules* **1989**, *22*, 4130.
(6) Swatloski, R. P.; Spear, S. K.; Holbrey, J. D.; Rogers, R. D. *J. Am. Chem. Soc.* **2002**, *124*, 4974.
(7) Swatloski, R. P.; Rogers, R. D.; Holbrey, J. D. WO Pat. 03/029329, 2003.
(8) Dadi, A. P.; Varanasi, S.; Schall, C. A. *Biotechnol. Bioeng.* **2006**, *95*, 904.
(9) Zhang, H.; Wu, J.; Zhang, J.; He, J. S. *Macromolecules* **2005**, *38*, 8272.
(10) Zhu, S. D.; Wu, Y. X.; Chen, Q. M.; Yu, Z. N.; Wang, C. W.; Jin, S. W.; Ding, Y. G.; Wu, G. *Green Chem.* **2006**, *8*, 325.
(11) Dadi, A. P.; Schall, C. A.; Varanasi, S. *Appl. Biochem. Biotechnol.* **2007**, *137*, 407.
(12) Li, C.; Knierim, B.; Manisseri, C.; Arora, R.; Scheller, H. V.; Auer, M.; Vogel, K. P.; Simmons, B. A.; Singh, S. *Bioresour. Technol.* **2010**, *101*, 4900.
(13) Barthel, S.; Heinze, T. *Green Chem.* **2006**, *8*, 301.
(14) Xie, H. L.; Shi, T. J. *Holzforschung* **2006**, *60*, 509.
(15) Fukaya, Y.; Hayashi, K.; Wada, M.; Ohno, H. *Green Chem.* **2008**, *10*, 44.
(16) Zhao, H.; Baker, G. A.; Song, Z. Y.; Olubajo, O.; Crittle, T.; Peters, D. *Green Chem.* **2008**, *10*, 696.
(17) Fort, D. A.; Remsing, R. C.; Swatloski, R. P.; Moyna, P.; Moyna, G.; Rogers, R. D. *Green Chem.* **2007**, *9*, 63.
(18) Kilpelainen, I.; Xie, H.; King, A.; Granstrom, M.; Heikkinen, S.; Argyropoulos, D. S. *J. Agric. Food Chem.* **2007**, *55*, 9142.
(19) Pu, Y. Q.; Jiang, N.; Ragauskas, A. J. *J. Wood Chem. Technol.* **2007**, *27*, 23.
(20) Zavrel, M.; Bross, D.; Funke, M.; Buchs, J.; Spiess, A. C. *Bioresour. Technol.* **2009**, *100*, 2580.
(21) Fahlen, J.; Salmen, L. *Biomacromolecules* **2004**, *6*, 433.
(22) Beckham, G. T.; Matthews, J. F.; Peters, B.; Bomble, Y. J.; Himmel, M. E.; Crowley, M. F. *J. Phys. Chem. B* **2011**, *115*, 4118.
(23) Gericke, M.; Schlufter, K.; Liebert, T.; Heinze, T.; Budtova, T. *Biomacromolecules* **2009**, *10*, 1188.
(24) Song, H. Z.; Niu, Y. H.; Wang, Z. G.; Zhang, J. *Biomacromolecules* **2011**, *12*, 1087.
(25) Remsing, R. C.; Hernandez, G.; Swatloski, R. P.; Massefski, W. W.; Rogers, R. D.; Moyna, G. *J. Phys. Chem. B* **2008**, *112*, 11071.
(26) Remsing, R. C.; Petrik, I. D.; Liu, Z.; Moyna, G. *Phys. Chem. Chem. Phys.* **2010**, *12*, 14827.
(27) Remsing, R. C.; Swatloski, R. P.; Rogers, R. D.; Moyna, G. *Chem. Commu* **2006**, 1271.
(28) Zhang, J. M.; Zhang, H.; Wu, J.; Zhang, J.; He, J. S.; Xiang, J. F. *Phys. Chem. Chem. Phys.* **2010**, *12*, 1941.
(29) Liu, H.; Sale, K. L.; Holmes, B. M.; Simmons, B. A.; Singh, S. *J. Phys. Chem. B* **2010**, *114*, 4293.
(30) Shen, T.; Langan, P; D., F. A.; Johnson, G. P.; Gnanakaran, S. *J. Am. Chem. Soc.* **2009**, *131*, 14786.
(31) Kahlen, J.; Masuch, K.; Leonhard, K. *Green Chem.* **2010**, *12*, 2172.
(32) Kirschner, K. N.; Woods, R. J. *Proc. Natl. Acad. Sci. U.S.A.* **2001**, *98*, 10541.
(33) Matthews, J. F.; Skopec, C. E.; Mason, P. E.; Zuccato, P.; Torget, R. W.; Sugiyama, J.; Himmel, M. E.; Brady, J. W. *Carbohydr. Res.* **2006**, *341*, 138.
(34) Yui, T.; Hayashi, S. *Biomacromolecules* **2007**, *8*, 817.
(35) Gross, A. S.; Chu, J. W. *J. Phys. Chem. B* **2011**, *114*, 13333.
(36) Gross, A. S.; Bell, A. T.; Chu, J.-W. *J. Phys. Chem. B* **2011**, *115*, 13433.
(37) Bellesia, G.; Chundawat, S. P. S.; Langan, P.; Dale, B. E.; Gnanakaran, S. *J. Phys. Chem. B* **2011**, *115*, 9782.
(38) Nishiyama, Y.; Sugiyama, J.; Chanzy, H.; Langan, P. *J. Am. Chem. Soc.* **2003**, *125*, 14300.
(39) DeLano, W. L. In *The PyMOL molecular Graphic System*, 2002; http://www.pymol.org.
(40) Nishiyama, Y.; Johnson, G. P.; French, A. D.; Forsyth, V. T.; Langan, P. *Biomacromolecules* **2008**, *9*, 3133.
(41) Martínez, L.; Andrade, R.; Birgin, E. G.; Martínez, J. M. *J. Comput. Chem.* **2009**, *30*, 2157.
(42) Case, D. A.; Darden, T. A.; Cheatham, I., T. E. ; Simmerling, C. L.; Wang, J.; University of California, San Francisco: 2006.
(43) Wang, J. M.; Wang, W.; Kollman, P. A.; Case, D. A. *J. Mol. Graphics Modell.* **2006**, *25*, 247.
(44) Woods, R. J.; Dwek, R. A.; Edge, C. J.; Fraserreid, B. *J. Phys. Chem.* **1995**, *99*, 3832.
(45) Darden, T.; York, D.; Pedersen, L. *J. Chem. Phys.* **1993**, *98*, 10089.
(46) Nishiyama, Y.; Langan, P.; Chanzy, H. *J. Am. Chem. Soc.* **2002**, *124*, 9074.
(47) Mason, P. E.; Neilson, G. W.; Enderby, J. E.; Saboungi, M. L.; Cuello, G.; Brady, J. W. *J. Chem. Phys.* **2006**, *125*, 9.

(48) Cheng, G.; Varanasi, P.; Li, C.; Liu, H.; Melnichenko, Y. B.; Simmons, B. A.; Kent, M. S.; Singh, S. *Biomacromolecules* **2011**, *12*, 933.
(49) Wada, M.; Ike, M.; Tokuyasu, K. *Polym. Degrad. Stab.* **2010**, *95*, 543.
(50) Driemeier, C.; Calligaris, G. A. *J. Appl. Crystallogr.* **2010**, *44*, 184.
(51) Thygesen, A.; Oddershede, J.; Lilholt, H.; Thomsen, A. B.; Stahl, K. *Cellulose* **2005**, *12*, 563.